1 **Chemical characteristics of submicron particles at the central**

2 **Tibet Plateau: influence of long-range transport**

3

4 Jianzhong Xu[1], Qi Zhang[2], Jinsen Shi[3], Xinlei Ge[4], Conghui Xie[1], Junfeng Wang[4],

5 Shichang Kang[1], Ruxiong Zhang[5], Yuhang Wang[5]

6

7 [1]State Key Laboratory of Cryospheric Sciences, Northwest Institute of Eco-Environment and Resources,

8 CAS, Lanzhou 730000, China

9 [2]Department of Environmental Toxicology, University of California, Davis, CA 95616, USA

10 [3]Key Laboratory for Semi-Arid Climate Change of the Ministry of Education, College of Atmospheric

11 Sciences, Lanzhou University, Lanzhou 730000, China

12 [4]Jiangsu Key Laboratory of Atmospheric Environment Monitoring and Pollution Control (AEMPC),

13 School of Environmental Science and Engineering, Nanjing University of Information Science &

14 Technology, Nanjing 210044, China

15 [5]School of Earth and Atmospheric Sciences, Georgia Institute of Technology, Atlanta, GA, USA

16

17 **Abstract**

18 Recent studies have revealed a significant influx of air pollution from south Asia to Himalayas and Tibet

19 Plateau (TP) during pre-monsoon period. In order to characterize the chemical composition, sources, and

20 transport mechanism of polluted air mass in this pristine area, we performed a field study during June 2015

21 by deploying a suite of online instruments including an Aerodyne high-resolution time-of-flight aerosol

22 mass spectrometer (HR-AMS) and a multi-angle absorption photometer (MAAP) at Nam Co Station

23 (90°57′E, 30°46′N 4730m a.s.l) at the central of the TP. The measurements were made at a time when the

24 transition from pre-monsoon to monsoon occurred. The average ambient mass concentration of submicron

25 particulate matter (PM$_1$) over the whole campaign period was 2.0 µg m^{-3}, with organics accounting for

26 64%, followed by sulfate (16%), black carbon (9%), ammonium (8%), and nitrate (3%). This mass loading

27 and composition were comparable with most of AMS results in remote sites worldwide. Air pollution

28 episodes were observed during the pre-monsoon period, while consistently low aerosol concentrations were

29 observed during the monsoon period. However, the chemical composition of aerosol during the air

30 pollution episodes in the pre-monsoon season was on a case-by-case basis, depending on the prevailing

31 meteorological conditions and air mass transport routes. Most of the chemical species exhibited significant

32 diurnal variations with higher values occurring during afternoon and lower values during early morning

33 time whereas nitrate peaked during early morning in association with higher relative humidity and lower air

34 temperature. Organic aerosol (OA) was more oxidized with an oxygen-to-carbon ratio (O/C) of 0.94 during

35 the pre-monsoon period than during monsoon (average O/C of 0.48). The average O/C of OA was 0.88

36 over the entire campaign period. Positive matrix factorization of the high resolution mass spectra of OA

37 identified two oxygenated organic aerosol (OOA) factors: a less oxidized OOA (LO-OOA) and a more

38 oxidized OOA (MO-OOA). The MO-OOA dominated during the pre-monsoon period, while LO-OOA

39 dominated during the monsoon. The sensitivity of air pollution transport with synoptic process was also

40 evaluated with a 3-D chemical transport model.

41

1. Introduction

43 The Tibet Plateau (TP) and Himalayas is a vast and elevated highland in Central Asia that extends over the

44 area of 27-45°N, 70-105°E with a mean elevation of more than 4000 m above sea level (a.s.l.). It is a

45 sparsely populated area with minimal local pollution. The TP is an ideal area for observations of free

46 tropospheric air masses and pollutants from polluted areas surrounding the TP after long-range transport.

47 Determination of the chemical characteristics of aerosol particles in TP is important for assessment on their

48 influence on atmospheric chemistry and climate (Li et al., 2016), which are so far poorly understood due to

49 harsh conditions and logistic limitation.

50

51 Over recent decades, an increasing number of field studies have been conducted in these regions to

52 characterize aerosol physical and chemical features from mountain observatories, e.g., the Nepal Climate

53 Observatory-Pyramid (5079 m), which are set up for long-term monitoring and synchronous observation

54 (Bonasoni et al., 2010; Liu et al., 2017). There are significant seasonal variations in aerosol loading in the

55 southern TP and Himalayas. Higher aerosol concentration was often found during pre-monsoon due to less

56 precipitation and favorable atmospheric circulation (Bonasoni et al., 2010; Marinoni et al., 2010; Marinoni

57 et al., 2013; Zhao et al., 2013). For example, the concentration of carbonaceous species at the Qomolangma

58 (Mt. Everest) Station (4276 m a.s.l.), northern Himalayas during pre-monsoon was found to be $3 - 5$ times

59 higher than that during the monsoon periods (Cong et al., 2015). Since this seasonal variation of aerosol

60 loading is consistent at both the southern and northern Himalayas (Xu et al., 2014), polluted air mass was

61 thought to be able to across the Himalayas, a condition which is also supported by model results (Lu et al.,

62 2012; Lüthi et al., 2015; Zhang et al., 2015). During monsoon period, ambient aerosol at the upwind

63 sources is significantly scavenged before long-range transport and air mass are mainly originated from

64 marine which had chemical difference between pre-monsoon and monsoon.

65

66 Most of the studies conducted in these regions focused on some specific species, such as black carbon,

67 which has strongly light absorption. Burning of biomass fuels and wildfires in the south Himalaya and

68 South Asia are thought to be important sources for the black carbon (Stone et al., 2010; Engling et al., 2011;

69 Kumar et al., 2011). However, a recent study shows that sources of black carbon in the region of South

70 Asia are highly complex, including emissions from low efficient transport tools and cooking using cow

71 dung and biogas as well (Stockwell et al., 2016). These burning activities also emit other species such as

72 organic and inorganic particulate species and volatile organic compounds, which generate a well-mixed

73   aerosol plume eventually via processes such as coagulation, evaporation, oxidation, and condensation. Fang

74   et al. (2015) recently suspected that biogenic aerosol could also be an important contribution for aerosol in

75   the TP during summer. However, these mixed plumes have been rarely, if ever, characterized by

76   comprehensive field measurements.

77

78   Filter-based sampling method with a low time resolution (days) were widely adopt in these remote regions

79   due to logistical difficulties with deployment of real-time instruments. The low time resolution made the

80   understanding of chemical processes of aerosol during transport challenging. Secondary species such as

81   sulfate and water soluble organic carbon (WSOC) are normally the dominated species in aerosol. For

82   example, WSOC accounted for about 60% of OC and the ratio between OC and EC could be up to 10

83   (Zhao et al., 2013; Cong et al., 2015), suggesting a dominant contribution of secondary organic aerosol

84   (SOA) to carbonaceous aerosol loading in the TP. The ambient conditions at high elevation regions are

85   characterized by higher solar radiation and concentrations of oxidants such as OH radicals and O_3, which

86   make photochemical processing in this high elevation remote region intense and likely dynamic. Therefore

87   high-resolution measurement is necessary in these regions for detecting short-term events and the evolution

88   of pollution events. In addition, the high time resolution data are useful for constraining atmospheric

89   chemical transport models.

90

91   The aerodyne aerosol mass spectrometer (AMS) has been widely used to study the chemical composition of

92   non-refractory submicron particle. There are two merits of the AMS including its high time resolution and

93   bulk measurement. The high time resolution is usually minute which has advanced our understanding of

94   fundamental chemical composition at different regions of the world (Canagaratna et al., 2007). The bulk

95   measurements make the observation obtain more information of aerosol in one time. The organic aerosol,

96   which is often the most important component of aerosol, can be further analyzed for their mass spectra to

97   determine the average elemental ratios and by positive matrix factorization (PMF) analysis to determine the

98   sources and atmospheric processes of aerosol (Ulbrich et al., 2009; Zhang et al., 2011). The atomic

99   elemental ratios of oxygen and hydrogen with carbon (O:C and H:C) calculated from the OA mass spectra

100 can provide information about the sources and evolution processes of OA in the atmosphere (Aiken et al.,

101 2008; Heald et al., 2010; Kroll et al., 2011; Ng et al., 2011). They also often correlate with key OA

102 properties such as hygroscopicity, material density, and phase separation (Jimenez et al., 2009; Bertram et

103 al., 2011). In addition, due to high sensitivity, AMS has been successfully deployed at many remote sites

104 with low aerosol loading such as Antarctica (Schmale et al., 2013; Giordano et al., 2017). However, there

105 are not AMS measurement in the TP and Himalayas so far.

106

107 The study here presents an analysis of comprehensive measurements using AMS acquired at the central of

108 the TP during the transitional season from pre-monsoon to monsoon. The study was designed to

109   characterize aerosol chemical composition, temporal variations, transport processes, and emission sources.

110   During the campaign, multiple real-time instruments were deployed.

111

112   **2. Methodology**

113   **2.1 Site description**

114   The field study was conducted between May 31 and July 1, 2015 at a high altitude observatory, i.e., Nam

115   Co Station for Multisphere Observation and Research, Chinese Academy of Sciences (Nam Co station,

116   90°57′E, 30°46′N 4730m a.s.l), at the central part of the TP (Figure 1). The Nam Co station is located

117   nearby Nam Co lake (Figure 1b), the second largest inland lake in the TP (area: 1920 km^2) which is located

118   at the northern border of Nyainqentanglha Mountains. The melted glacier from Nyainqentanglha Mountains

119   supply water to the lake each year during warm seasons. This is a pristine region except for a small county

120   for local people that is about 10 km to west of the station. In the past several years, tourism for this

121   beautiful lake has growth. A highway for tourists was built about 1 km south of the station. The capital city

122   (Lhasa) of the Tibet Autonomous Region is about 100 km southeast of the station with an average elevation

123   of 3600 m a.s.l. between which is Nyainqentanglha Mountains (higher than 6000 m a.s.l) (Figure 1c). The

124   closest town, Dangxiong, is along the famous highway, Qinghai-Tibet Highway, and about 70 km east of

125   the station with an average elevation of 4200 m a.s.l. Overall, the station is around by the mountains in the

126   south and east, and the lake at the west. The ecology of surrounding area is semi-arid type land dominated

127   by alpine meadow and barren areas. The precipitation is mainly occurred during summer monsoon period.

128   The cooking and heating at the station is maintained by the power and natural gas.

129

130   **2.2 Instrument setup**

131   The study was conducted at the observatory field of the station using a customer-made trailer with inlet

132   stepped out of the top with the height of ~5m above ground. All the instruments were arranged in the trailer

133   where the air temperature is controlled at 20°C by two conditions. Figure 1 shows the set-up of the

134   instruments. The total inlet was maintained by a vacuum pump with a flowrate of 10 m/s, following by a

135   high-resolution time-of-flight aerosol mass spectrometer (HR-AMS, Aerodyne Research Inc., Billerica,

136   MA, USA), a custom-made scanning mobility particle sizer (SMPS), a soot particle Aerodyne mass

137   spectrometer (SP-AMS, Aerodyne Research Inc., Billerica, MA, USA), a single-particle intracavity laser-

138   induced incandescence photometer (SP2, DMT, Inc., Boulder, CO, USA), and a seven wavelength

139   Athelometer (model AE31, Magee Scientific, Berkeley, CA, USA). The total flowrate of this inlet was

140   maintained at ~16 m/s and a $PM_{2.5}$ cyclone at the beginning of the inlet (model URG-2000-30EH, URG

141   Corp., Chapel Hill, NC, USA). Several additional instruments were also co-located with their own inlet,

142   such as a Nephelometer (model 3563, TSI, Shoreview, MN, USA), a $PM_{2.5}$ sampler (model PQ200, BGI,

143   USA), and a multi-angle absorption photometer (MAAP, model 5012, Thermo Electron Cooperation, USA).

144   The operations of the instruments used in this study were described below.

145

146 2.2.1 HR-AMS

147 HR-AMS was used to measure non-refractory PM_1 (NR-PM_1) which was thermal vaporized at ~600 °C,

148 ionized with a 70eV electron impact and measured using a time of flight mass spectrometry. The details on

149 the instrument have been described elsewhere (DeCarlo et al., 2006). For this study, HR-AMS was only

150 setup with V-mode with 5 min resolution due to the low aerosol loading. Due to damage of chopper, the

151 size distribution of NR-PM_1 was not determined. The HR-AMS was calibrated for ionization efficiency (IE)

152 with the ammonium nitrate following standard procedures (Jayne et al., 2000) at the beginning, in the

153 middle and end of the study. Particulate-free air was sampled two times during the study to adjust the

154 interaction of air on the fragmentation table and the detection limitation (DLs) of species. The DLs were

155 calculated as 3 times the standard deviations (3σ) of the measured values during this period. The 2.5-min

156 DLs for organic, sulfate, nitrate, ammonium, and chloride were determined at 0.108, 0.014, 0.007, 0.002,

157 0.010, which are comparable to the values reported in previous studies.

158

159 2.2.2 Other instruments

160 The Aethalometer was used to measure the equivalent black carbon mass concentration using seven

161 wavelength lights. The data for BC is commonly calculated from measurement at 880 nm using

162 recommended MAC from factory. The instrument was operated at the time resolution of 5 min with a flow

163 rate of 5 L/min, which was calibrated at a week frequency.

164

165 $PM_{2.5}$ sampler was operated at the top of the trailer. Filter samples were collected between 2 June and 1

166 July 2015. Each aerosol sample was collected on a 47 mm quartz filter (Whatman, Maidstone, UK) using

167 the aerosol sampler. The meteorological data was recorded at the tower of the Nam Co station at a height of

168 20 m above ground.

169

170 **2.3 Data processing**

171 The HR-ToF-AMS data were processed using the standard software of SQUIRREL (v1.56) and PIKA

172 (v1.15c) (http://cires.colorado.edu/jimenez-group/ToFAMSResources/ToFSoftware/index.html) to

173 determine the mass concentrations of the NR-PM_1 species and the ion-speciated mass spectra of organics,

174 written in IGOR (Wavemetrics, Inc., Lake Oswego, OR, USA). An empirical particle collection efficiency

175 (CE) of 0.5 was used, which has been widely used in field studies employing AMS with a dryer installed in

176 front of the equipment's particle inlet. This CE value was further validated by the consistency and

177 reasonable slope between HR-AMS measured mass concentrations and SMPS-determined particle volumes

178 (section 3.1.2, R^2 = 0.9, slope = 1.48). The elemental ratios of OA (O:C, H:C, and organic matter to carbon

179 (OM:OC)) for this study was determined using the "improved-ambient" method (Canagaratna et al., 2015).

180

181 The source decomposition of organics was analysed by PMF with the robust engine. First, organic matrix

182 was analysed using the PMF2.exe algorithm in robust mode (Paatero and Tapper, 1994) and explored using

Atmospheric
Chemistry
and Physics
Discussions

183   the PMF Evaluation Toolkit (PET) (Ulbrich et al., 2009). The PMF solution was evaluated following the

184   procedures outlined in Table 1 of (Zhang et al., 2011) including modification of the error matrix and

185   downweight of low S/N ions. Moreover, based on the AMS fragmentation table, some organic ions were

186   not directly measured but scaled to the organic signal at m/z 44, which were downweighted by increasing

187   their errors by a factor of 3. A two-factor solution with fPeak = 0 was chosen in this study, as it is able to

188   reconstruct the total OA mass and temporal profiles very well. The results of three-factor solution with

189   fPeak = 0 are shown in supplementary material (Figure S1), which show splitting in the solutions.

190

191   3 Results and discussions

192   3.1 The meteorological conditions during the study

193

194   During the field study, the meteorological conditions were generally cold and windy (Figure 2a and b). The

195   average air temperature was 8.4 ± 3.6 °C with a diurnal hourly average ranging from 4.8 to 12.3 °C; the

196   diurnal average wind speed (WS) ranged from 4.5 to 6.5 m s^{-1}. The dominant wind direction was south and

197   southwest, although it varied during different periods (Figure 2b and S2). The wind direction (WD) had

198   distinct diurnal variation with air mass from south during night to morning and west during afternoon.

199   Based on the report of the Climate Diagnostics Bulletin of India

200   (http://imdpune.gov.in/Clim_RCC_LRF/Climate_Diagnostic_Bulletins/cdbi_apr_2015.pdf), the

201   precipitation from Indian monsoon had covered most part of India on June 12 to June 14, and these days

202   are treated as the onset of India monsoon. Indeed, precipitation was recorded at the Nam Co station on June

203   13 and lasted for several days (Figure 2a). Based on this weather condition, the period before June 14 was

204   classified as the pre-monsoon period and afterwards as the monsoon period. The RH during the pre-

205   monsoon and monsoon periods were 48.4 ± 19.2% and 58.8 ± 16.5%, respectively. The originations of the

206   air masses were also different during these two periods. Figure 3 shows the air mass from west during pre-

207   monsoon periods accounted about 30-40%, while it was only 7% during monsoon period of which ~80%

208   was from south.

209

210   3.2 The temporal variation of chemical species

211

212   The average mass concentration of PM$_1$ (NR-PM$_1$ + BC) was 2.0 μg m^{-3} during the whole study period

213   with 68% OA, 15% sulfate, 2% nitrate, 7% ammonium, and 8% BC. The NR-PM$_1$ loading (1.84 μg m^{-3}) at

214   Nam Co Station was lower than the values observed at some high elevation sites such as Menyuan (10.8 μg

215   m^{-3}) (Du et al., 2015), Montsec (4.9 μg m^{-3}) (Ripoll et al., 2015), Mt. Cimone (4.5 μg m^{-3}) (Rinaldi et al.,

216   2015), Puy de Done (5 – 27 μg m^{-3}), and Mt. Bachelor (15.1 μg m^{-3}) (Zhou et al., 2017), but higher than

217   some other sites, such as sub-Antarctic (0.46 μg m^{-3}) (Schmale et al., 2013) and Jungfraujoch (0.55 μg m^{-3})

218   (Fröhlich et al., 2015), similar with that at Mt. Whistler (1.91 μg m^{-3}) (Sun et al., 2009) (Table 1 and Figure

219   S3). Although the sampling season and elevation of these sampling sites are different (Table 1), the results
220   of these studies could basically represent the level of pollution at these sits due to their relatively long
221   sampling spans (from one month to ten months). The contribution of OA at these high-elevation sites
222   ranged from 50% − 90%; the highest value was at Mt. Bachelor which was frequently influenced by
223   transported biomass burning plume, while the relative low OA contribution (38%) at sub-Antarctic was due
224   to the dominant source from marine emission containing higher sulfate. The mass concentration of PM_1
225   varied dynamically during the study with distinct difference between pre-monsoon and monsoon periods.
226   The average mass concentrations of PM_1 for these two periods were 2.6 and 1.2 µg m^{-3}, respectively. For
227   comparison, the chemical species for these two periods were side-by-side displayed in Figure 4a. The ratios
228   between pre-monsoon and monsoon for all the species were higher than 1 with the maxima for ammonium
229   (3.1) and sulfate (2.8), suggesting high efficiency of wet scavenging for ammonium sulfate during monsoon.
230   The contribution of OA was thus slightly higher during the monsoon period than during the pre-monsoon
231   (71% vs. 64%).

233   Based on the mass concentration and temporal variations of PM_1 species and weather conditions, the pre-
234   monsoon period could be further divided into two, i.e., period 1 (P1: May 30 to June 7) and period 2 (P2:
235   June 8 to June 13). The P1 was characterized by higher sulfate concentration (0.46 vs. 0.41 µg m^{-3}) and
236   sunny days, while P2 was characterized by higher PM_1 concentration (2.9 vs. 2.1 µg m^{-3}), higher nitrate
237   contribution, and wet and cold days (Figure S4). The air masses for P2 had higher contribution from west
238   and north than those during P1 (Figure 3). Figure 4b shows the comparisons of mass concentration of
239   different species between these two periods. For chemical species, from P1 to P2, nitrate and OA increased
240   dramatically by a factor of 1.6 and 2.2, respectively, and BC and ammonium were also increased,
241   suggesting the influence of transported polluted air mass. However, sulfate and chloride decreased slightly
242   (the ratios between P1 and P2 were ~0.95). The variations of sulfate and nitrate during these two periods
243   could be related to the photochemical conditions and origination of air mass (see section 3.3).

245   The particles were generally chemical neutralized as illustrated from the scatter plot between predicted and
246   measured ammonium (slope = 0.91) (Figure S5a). The neutralized PM_1 were likely due to the high
247   availability of ammonia from agriculture emission in North of India (Clarisse et al., 2009; Van Damme et
248   al., 2015). The slope was ~0.75 during P2 (Figure S5a), which suggested that there was over ammonium to
249   neutralize sulfate and nitrate. We check whether the high concentration of ammonium was from
250   fragmentation of organic nitrogen such as amine, however, the ratios of NH^+ and NH_2^+ were consistently
251   during the study (Figure S5b), suggesting there was no amine compounds. This high contribution from
252   ammonium could be related to the presence of significant amounts of organic anions in aerosol (such as
253   carboxylic acids) or variation of RIE for ammonium.

254

Atmospheric
Chemistry
and Physics
Discussions

Open Access

3.3 Diurnal variation and chemical process of different species

The diurnal variation of OA, sulfate, nitrate, ammonium, and BC during different periods are shown in Figure 5. All these species unexpected present significant diurnal patterns, especially during P2. The diurnal variation of aerosol are usually related to the local source emission (e.g., Xu et al., 2016). The diurnal variation at Nam Co may be related to the diurnal variations of long-range transport air mass, photochemistry, and the variation of plenary boundary layer (PBL). OA, sulfate, ammonium, and BC showed a similar pattern with low values during nighttime to early morning and high values during afternoon. We check the diurnal variation of the origination of air masses and found that there were increased air masses from south during nighttime and from west during afternoon (Figure S6), which could be related to the plateau monsoon during summer (Tang and Reiter, 1984). The enhanced air mass from west during afternoon could be more favorable for transport polluted air mass. The diurnal variations of chemical species during monsoon period were relatively flat comparing with those during P1 and P2. Nitrate presented a significant different diurnal variation with high values during nighttime to early morning and low values during afternoon. These features were highly correlated with that of RH and air temperature (Figure 5) suggesting the important chemical processing of particle/gas partitioning of ammonium nitrate and hydrolysis of N_2O_5. In addition, during early morning time (6:00 – 8:00), there were a peak for most of species, which were corresponding with the lowest air temperature and the highest RH, then lower PBL which could concentrate all the polluted air in a smaller space (Yanai and Li, 1994).

Although the diurnal patterns for each species were similar during the three periods, the relationships of chemical species with wind conditions were significant different based on bivariate polar plot analysis (Figure 6). Sulfate and ammonium during P1 had hotspots from all of the directions at a big range of wind speed (0 – 10 m s^{-1}) suggesting the local/regional transport and formation of ammonium sulfate from different air mass; while OA were concentrated depending to the prevailing wind direction from southeast and northwest suggesting important transport routes for OA from these two directions; nitrate had hotspots at the lowest wind speed (0 – 8 m s^{-1}) only from southwest suggesting the nearby sources and/or local formation; while BC had hotspots from south, west and northwest at high wind speed (4 – 12 m s^{-1}) during P1 suggesting long-range transport from the concentrated polluted regions in northern India and northwestern India. During P2, all species except nitrate had hotspots from south at high wind speed (6 – 14 m s^{-1}), suggesting the different synoptic process comparing with that during P1. Nitrate still had hotspots at a relative low wind speed from southwest during P2. These results suggested that the sources and chemical formation for P1 and P2 were similar, albeit the wind conditions were different. During monsoon period, all species had more similar distribution of hotspots and strongly from northwest and weakly form southeast.

Atmospheric
Chemistry
and Physics
Discussions

291 The significant difference of diurnal variation between sulfate and nitrate suggested the different chemical
292 evolution of these two species. Nitrate and sulfate during three periods all had weak correlations. During P1,
293 the ratios of sulfate versus nitrate had peaks (> 20) during afternoon time, while during P2, the ratios all
294 kept at low values (< 20) (not shown). In order to further check on the chemical evolutions of these two
295 species, we dig out the high concentration periods based on nitrate concentration (> average + 2σ). Figure 7
296 showed all periods during the high nitrate period of the study and the corresponding meteorological
297 conditions. It is easy to find that most of the high loading periods occurred during the nighttime. The wind
298 speed and wind direction were varied dynamically and most of them were from southwest. Higher wind
299 speed from this wind direction could transport more polluted air mass to Nam Co as illustrated from the
300 event 1 (E1) during which all the species (OA, sulfate, ammonium, and BC) except nitrate increased; the
301 weather during this type event was accompanied with warm and dry air conditions. While when the wind
302 direction was from southwest with lower wind speed (E2), the RH increased to higher than 90%
303 accompanying deceased air temperature, and the mass concentrations of nitrate, sulfate and OA increased
304 significantly and BC decreased in contrast with the increase of nitrate being the most significant. The
305 decreased mass concentration of BC indicated no primary aerosol transportation, thus the increased species
306 were mainly secondary formation.

307

3.4 The average chemical feature of organic aerosol

309

310 The average mass spectrum of OA was shown in Figure 8a. The organic mass was on average composed of
311 51% oxygen, 44% carbon, and 5% hydrogen with an average nominal formula being $C_1H_{1.33}O_{0.88}N_{0.001}$. On
312 average, $C_xH_yO_1^+$ (38.1%) and $C_xH_y^+$ (37.3%) ions dominated the total OA following by $C_xH_yO_2^+$ (19.8%),
313 and $H_yO_1^+$ (4.6%). m/z 44 was the base peak in the OA spectrum and mainly composed of CO_2^+ (99%). m/z
314 43 had a significant contribution from $C_2H_3O^+$ (82%) and $C_3H_7^+$ (18%). m/z 55, likely an important primary
315 fragment consisted of 51% $C_4H_7^+$ and 49% $C_3H_3O^+$. The OA was highly oxidized with O/C of 0.88 on
316 average. The OA was more oxidized during pre-monsoon than monsoon with higher O : C ratio (0.90 vs.
317 0.98) and lower H : C ratio (1.30 vs. 1.27) (Figure 8b). The oxidation states of OA during two pre-monsoon
318 periods were also different. The O/C during P2 (0.98) was higher than P1 (0.90) and the H/C was higher
319 during P1 than P2. Correspondingly, the OA during P2 was containing higher contribution of $C_xH_yO_1^+$
320 (40.3 vs. 39.1%) and $C_xH_yO_2^+$ (25.2 vs. 23.6%) ions than those of P1 (Figure 8c).

321

322 The diurnal variations of both O : C and OM : OC ratios presented higher values during late morning to
323 afternoon and lower values during early morning (Figure 9a). H : C presented an opposite trend. These
324 patterns suggested that OA was more oxidized during daytime which could be due to photo oxidation
325 and/or transport of highly oxidized OA during daytime. We check the variation of elemental ratios at the
326 function of OA mass and found that the O : C increased significantly accompanied with the increase of OA
327 mass concentration (Figure 9b). This result likely suggested the importance of transportation on the

Atmospheric
Chemistry
and Physics
Discussions

328 oxidized OA. However it was not possible that the polluted air mass arrived at Nam Co within several

329 hours due to the long distance from source regions (more than 1000 km from India). Previous studies have

330 reported the presence of an aerosol layer between 6 − 18 km a.s.l altitude over the Tibet Plateau during

331 summer (Tobo et al., 2007; Vernier et al., 2011). He et al. (2014) examined the vertical profiles of aerosol

332 extinction coefficients measured with a Micro Pulse Lidar at Naqu, about 100 km east of Nam Co Station,

333 and observed a maximum in aerosol extinction coefficient between 18 − 19 km a.s.l during summer 2011.

334 Recently, Gu et al. (2016) examined the chemical compositions using the global three-dimensional

335 Goddard Earth Observing System chemical transport model (GEOS-Chem) and found elevated aerosol

336 concentrations of sulfate, nitrate, ammonium, BC, and organic carbon over the TP. Further, observational

337 and modeling studies have also shown that deep convection over the Tibet Plateau during daytime which is

338 one of the important routes for tropospheric and stratospheric exchange (Cristofanelli et al., 2009;

339 Cristofanelli et al., 2010; Lin et al., 2016). Thus the enhanced aerosol during afternoon could possible from

340 the mixed downward of aerosol layer at 16 − 18 km altitude during the growth of boundary layer. This type

341 of transportation could not be captured by the re-analysis data used in the back-trajectory analysis likely

342 due to the low time and spatial resolution. The need further validation in the future in this region.

343

3.5 The PMF decomposition on the OA

345

346 The two OA factors determined by PMF have distinctly different mass spectra and diurnal patterns (Figure

347 10), including a less oxidized OOA (LO-OOA; O : C = 0.49) and a more oxidized OOA (MO-OOA; O : C

348 = 0.96). Both factors appeared to be secondary in nature. Our inability to separate an HOA factor is

349 consistent with the fact that $C_4H_9^+$ was a minor peak in the OA spectra (0.6% of the total signal) and the

350 average organic-equivalent concentration of $C_4H_9^+$ was only 0.008 μg m^{-3} during this study (Figure 5a).

351 Collier et al. (2015) reported that the average $fC_4H_9^+$ (fraction of total organic signal accounted for by

352 $C_4H_9^+$) was 8.1% in the mass spectrum of POA from vehicle emissions. Based on this relationship, even

353 assuming $C_4H_9^+$ was completely contributed by primary OA (POA) from vehicle emissions, the average

354 HOA concentration would be only ~ 0.1 ug m^{-3}, or 7% of total OA mass, during this study. Note that in this

355 study, $C_4H_9^+$ was fit well in the PMF analysis with very small residual, indicating that the signal of this ion

356 was properly apportioned between the two OOA factors.

357

358 The mass spectra of MO-OOA and LO-OOA were characterized by high peaks at m/z 44 (mostly CO_2^+)

359 and LO-OOA had a large peak at m/z 43 (mostly $C_2H_3O^+$) as well (Figure 10a). The contributions of the

360 $C_xH_yO_2^+$ ion category in these two mass spectra were 15.1% and 28.6%, respectively, while the

361 contributions of $C_xH_yO_1^+$ were 37.8% and 41.5%, respectively. The time series of LO-OOA correlated well

362 with $C_xH_yO_1^+$ and $C_xH_y^+$ ions, while MO-OOA correlated well with $C_xH_yO_2^+$ ions (Figure S7). In addition,

363 the time series of MO-OOA correlated well with sulfate (R^2 = 0.55), BC (R^2 = 0.54) and less well with

364 nitrate (R^2 = 0.33), while LO-OOA correlated poorly with sulfate, BC and nitrate (Figure 10b and S8).

365   These results highlight the oxidation degree of MO-OOA and LO-OOA. LO-OOA and MO-OOA

366   accounted for 41% and 59% on average, respectively, of total OA mass during this study (Figure 11a), and

367   their relative contributions varied across the study (Figure 2e). For example, LO-OOA accounted for 41%

368   of the total OA mass during P1 of the pre-monsoon period, 24% during P2, and 67% during the monsoon

369   period (Figure 11b). The diurnal pattern of MO-OOA was characterized by higher concentrations during

370   afternoon similar to those of sulfate and BC. While the diurnal pattern of LO-OOA peaked at early evening

371   time (Figure 10c). The polar plot showed concentrated hotspots to the northwest of the sampling site for

372   MO-OOA, and southeast for LO-OOA (Figure 6), indicating that the sources of these two components were

373   totally different. MO-OOA was likely closely related to long-range transport of air mass from South Asia,

374   while LO-OOA could from relative shorter distance transport such as marine air mass and regional

375   background aerosol during the nighttime. Shen et al. (2015) reported that there were significant aerosol

376   source from biogenic emission during summer near the Nam Co Station. As shown in Figure 12a and b,

377   MO-OOA, which was highly oxidized (O : C = 0.96), appeared on the up-left corner of the triangle plot

378   while LO-OOA was in the middle part with an O:C ratio of 0.49. The high oxidation degree of MO-OOA

379   was likely related to extensive aging processes occurred during long-range transport. The slope of linear

380   fitting of all the data points in V-K diaphragm is –0.76 suggesting the evolution of OA as carboxylic acid

381   functionalization (Figure 12c).

382

383   Biomass burning emission is an important source in South Asia and could be transported to Himalayas and

384   TP during pre-monsoon (Engling et al., 2011; Kumar et al., 2011; Sang et al., 2013; Cong et al., 2015),

385   however there are not evidently signals of biomass emitted aerosol in our AMS results such as signals at

386   m/z 60 and 73 in mass spectrum of OA which were found to be associated with levoglucosan formed from

387   the pyrolysis of cellulose (Alfarra et al., 2007). The contribution of f60 (fraction of total organic signal

388   accounted for by m/z 60) for LO-OOA and MO-OOA were 0.2% and 0.3%, respectively, which were

389   similar with the global background level (less than 0.3%) suggested by Cubison et al. (2011). These results

390   suggest that OA, if ever partly originated from biomass burning emission, could have been highly oxidized

391   during transport. This behavior had been observed in a few studies that levoglucosan could be quickly

392   (within a few hours) oxidized after being emitted (Ortega et al., 2013). In addition, Zhou et al. (2017)

393   recently reported the observation of a highly aged BBOA factor with *f60 < 0.3%* in its mass spectrum, in

394   aged wildfire plumes that had gone through extensive photochemical oxidation.

395

396   ## 3.6 Sensitivity of the chemical characteristics of PM_1 to synoptic process

397

398   Synoptic process is an important factor determining if the regional emissions can be transported to the TP.

399   It is interesting to know what kind of synoptic process is favorable for transporting the polluted air mass to

400   the Himalayas and the TP. A 3-D Regional chemical transport Model (REAM) coupled with the Weather

401   Research and Forecasting model (WRF) was used to examine the chemical evolution and regional transport

402   of pollutants such as aromatics in this study. REAM has been used in previous studies of the Tibet Plateau,

403   and details about the model can be found in Zhang et al. (2017) and supplementary material. REAM could

404   capture some synoptic processes which cannot be simulated by the normally used reanalysis data due to

405   their low-resolution and the complexity of terrain in the Tibet Plateau (Zhang et al., 2017). Figure 13

406   shows the distribution of simulated daily surface wind, 300 hPa geopotential height fields and

407   concentrations of reactive aromatics over the Tibetan Plateau during 30 May – 13 June, 2015. During 30

408   May to 7 June corresponding to P1 in this study, there was a trough over the north propagated from west to

409   east and this low pressure induced increasingly stronger surface wind from India to the TP, which could

410   lead to transport of polluted air mass as illustrated by the results of model and AMS. The simulated

411   concentration of reactive aromatics showed a peak during this period (Figure S9). During 8-11 June, there

412   was a weak ridge system over the north. Intensified wind from north was observed as illustrated by

413   HYSPLIT results (Figure 5b) and the simulated concentrations of reactive aromatics were sharply

414   decreased (Figure S9). After that, a weak low-pressure trough system was observed again. The increased

415   concentrations of reactive aromatics were also observed accompanying with intensified southern wind.

416   These trends were basically consistent with that AMS results. The potential reason for this difference was

417   that the weak trough during P2 intensified the wind from west other than south where a lot of biomass

418   burning emission sources were located (Figure 5b). Meanwhile the interaction between cold-dry air mass

419   from north and warm-wet air mass from south increased the RH at Nam Co which was very favorable for

420   aqueous formation. Zhang et al., (2017) suggested that a low-cut system from stratosphere could be an

421   important driver for pollution transport into the Tibet Plateau. However, this effect tends to be weaker in

422   summer than in the other seasons because the tropopause is higher and stratospheric wave activity is

423   weaker in summer. In our study, the trough/ridge system could be an important factor affecting on the

424   transport of air pollution from south and west.

425

4. Conclusion

427

428   The average PM_1 loading measured at Nam Co during June 2015 was 2.0 μg m^{-3} with organics accounting

429   for 68%, followed by sulfate (15%), black carbon (8%), ammonium (7%), and nitrate (2%). This mass

430   concentration was comparable to some AMS observations from mountain-top sites. The mass concentration

431   of PM_1 varied during different weather conditions with higher concentration during pre-monsoon and lower

432   concentration during monsoon. The pre-monsoon period could also be divided into two periods (P1 and P2)

433   based on meteorological conditions and aerosol chemical composition. During P1, PM_1 was characterized

434   with high contribution from OA and sulfate, while increased contribution of nitrate was observed during P2

435   with wet and cold weather conditions. All PM_1 species had clear diurnal variations with OA, sulfate, BC,

436   and ammonium peaking during afternoon due to photochemical production of these species coupled with

437   transport of polluted air mass. Nitrate, however, peaked during the nighttime and early morning, which was

438   related to the higher RH condition. The formation of nitrate was highly correlated with transport of air

Atmospheric
Chemistry
and Physics
Discussions

439 masses from southwest under very low wind speeds, while the mass concentrations of sulfate, OA, and BC

440 were highly correlated with air masses from northwest and southeast under higher wind speed conditions.

441 OA was overall highly oxidized during the entire study with higher O/C ratios during the pre-monsoon

442 period. Based on PMF analysis, the OA was found to be composed of a LO-OOA and a MO-OOA. LO-

443 OOA was mainly associated with air masses originated from south, while MO-OOA was mainly from

444 northwest. MO-OOA dominated OA during the pre-monsoon period, while LO-OOA dominated during the

445 monsoon period. The transport mechanism of polluted air plume was further checked using the REAM

446 chemical model coupled with the WRF model. The polluted air plume was found to be more easily

447 transported to the TP and Himalayas during low pressure trough weather.

448

449 **Acknowledgements**

450

Atmospheric
Chemistry
and Physics
Discussions

Reference:

Aiken, A. C., DeCarlo, P. F., Kroll, J. H., Worsnop, D. R., Huffman, J. A., Docherty, K. S., Ulbrich, I. M., Mohr, C., Kimmel, J. R., Sueper, D., Sun, Y., Zhang, Q., Trimborn, A., Northway, M., Ziemann, P. J., Canagaratna, M. R., Onasch, T. B., Alfarra, M. R., Prevot, A. S. H., Dommen, J., Duplissy, J., Metzger, A., Baltensperger, U., and Jimenez, J. L.: O/C and OM/OC Ratios of Primary, Secondary, and Ambient Organic Aerosols with High-Resolution Time-of-Flight Aerosol Mass Spectrometry, Environ. Sci. Technol., 42, 4478-4485, 10.1021/es703009q, 2008.

Alfarra, M. R., Prevot, A. S. H., Szidat, S., Sandradewi, J., Weimer, S., Lanz, V. A., Schreiber, D., Mohr, M., and Baltensperger, U.: Identification of the Mass Spectral Signature of Organic Aerosols from Wood Burning Emissions, Environ. Sci. Technol., 41, 5770-5777, 10.1021/es062289b, 2007.

Bertram, A., Martin, S., Hanna, S., Smith, M., Bodsworth, A., Chen, Q., Kuwata, M., Liu, A., You, Y., and Zorn, S.: Predicting the relative humidities of liquid-liquid phase separation, efflorescence, and deliquescence of mixed particles of ammonium sulfate, organic material, and water using the organic-to-sulfate mass ratio of the particle and the oxygen-to-carbon elemental ratio of the organic component, Atmos. Chem. Phys., 11, 10995-11006, 10.5194/acp-11-10995-2011, 2011.

Bonasoni, P., Laj, P., Marinoni, A., Sprenger, M., Angelini, F., Arduini, J., Bonafè, U., Calzolari, F., Colombo, T., Decesari, S., Di Biagio, C., di Sarra, A. G., Evangelisti, F., Duchi, R., Facchini, M. C., Fuzzi, S., Gobbi, G. P., Maione, M., Panday, A., Roccato, F., Sellegri, K., Venzac, H., Verza, G. P., Villani, P., Vuillermoz, E., and Cristofanelli, P.: Atmospheric Brown Clouds in the Himalayas: first two years of continuous observations at the Nepal Climate Observatory-Pyramid (5079 m), Atmos. Chem. Phys., 10, 7515-7531, 10.5194/acp-10-7515-2010, 2010.

Canagaratna, M. R., Jayne, J. T., Jimenez, J. L., Allan, J. D., Alfarra, M. R., Zhang, Q., Onasch, T. B., Drewnick, F., Coe, H., Middlebrook, A., Delia, A., Williams, L. R., Trimborn, A. M., Northway, M. J., DeCarlo, P. F., Kolb, C. E., Davidovits, P., and Worsnop, D. R.: Chemical and microphysical characterization of ambient aerosols with the aerodyne aerosol mass spectrometer, Mass. Spectrom. Rev., 26, 185-222, 10.1002/mas.20115, 2007.

Canagaratna, M. R., Jimenez, J. L., Kroll, J. H., Chen, Q., Kessler, S. H., Massoli, P., Hildebrandt Ruiz, L., Fortner, E., Williams, L. R., Wilson, K. R., Surratt, J. D., Donahue, N. M., Jayne, J. T., and Worsnop, D. R.: Elemental ratio measurements of organic compounds using aerosol mass spectrometry: characterization, improved calibration, and implications, Atmos. Chem. Phys., 15, 253-272, 10.5194/acp-15-253-2015, 2015.

Clarisse, L., Clerbaux, C., Dentener, F., Hurtmans, D., and Coheur, P.-F.: Global ammonia distribution derived from infrared satellite observations, Nature Geosci., 2, 479-483, 10.1038/ngeo551, 2009.

Collier, S., Zhou, S., Kuwayama, T., Forestieri, S., Brady, J., Zhang, M., Kleeman, M., Cappa, C., Bertram, T., and Zhang, Q.: Organic PM Emissions from Vehicles: Composition, O/C Ratio, and Dependence on PM Concentration, Aerosol. Sci. Tech., 49, 86-97, 10.1080/02786826.2014.1003364, 2015.

Cong, Z., Kang, S., Kawamura, K., Liu, B., Wan, X., Wang, Z., Gao, S., and Fu, P.: Carbonaceous aerosols on the south edge of the Tibetan Plateau: concentrations, seasonality and sources, Atmos. Chem. Phys., 15, 1573-1584, 10.5194/acp-15-1573-2015, 2015.

Cristofanelli, P., Bonasoni, P., Bonafé, U., Calzolari, F., Duchi, R., Marinoni, A., Roccato, F., Vuillermoz, E., and Sprenger, M.: Influence of lower stratosphere/upper troposphere transport events on surface ozone at the Everest-Pyramid GAW Station (Nepal): first year of analysis, International Journal of Remote Sensing, 30, 4083-4097, 10.1080/01431160902821940, 2009.

Cristofanelli, P., Bracci, A., Sprenger, M., Marinoni, A., Bonafè, U., Calzolari, F., Duchi, R., Laj, P., Pichon, J. M., Roccato, F., Venzac, H., Vuillermoz, E., and Bonasoni, P.: Tropospheric ozone variations at the Nepal Climate Observatory-Pyramid (Himalayas, 5079 m a.s.l.) and influence of deep stratospheric intrusion events, Atmos. Chem. Phys., 10, 6537-6549, 10.5194/acp-10-6537-2010, 2010.

Cubison, M. J., Ortega, A. M., Hayes, P. L., Farmer, D. K., Day, D., Lechner, M. J., Brune, W. H., Apel, E., Diskin, G. S., Fisher, J. A., Fuelberg, H. E., Hecobian, A., Knapp, D. J., Mikoviny, T., Riemer, D., Sachse, G. W., Sessions, W., Weber, R. J., Weinheimer, A. J., Wisthaler, A., and Jimenez, J. L.: Effects of aging on organic aerosol from open biomass burning smoke in aircraft and laboratory studies, Atmos. Chem. Phys., 11, 12049-12064, 10.5194/acp-11-12049-2011, 2011.

Atmospheric
Chemistry
and Physics
Discussions

511   DeCarlo, P. F., Kimmel, J. R., Trimborn, A., Northway, M. J., Jayne, J. T., Aiken, A. C., Gonin, M., Fuhrer,
512   K., Horvath, T., Docherty, K. S., Worsnop, D. R., and Jimenez, J. L.: Field-Deployable, High-
513   Resolution, Time-of-Flight Aerosol Mass Spectrometer, Anal. Chem., 78, 8281-8289,
514   10.1021/ac061249n, 2006.
515   Du, W., Sun, Y. L., Xu, Y. S., Jiang, Q., Wang, Q. Q., Yang, W., Wang, F., Bai, Z. P., Zhao, X. D., and
516   Yang, Y. C.: Chemical characterization of submicron aerosol and particle growth events at a
517   national background site (3295 m a.s.l.) on the Tibetan Plateau, Atmos. Chem. Phys., 15, 10811-
518   10824, 10.5194/acp-15-10811-2015, 2015.
519   Engling, G., Zhang, Y.-N., Chan, C.-Y., Sang, X.-F., Lin, M., Ho, K.-F., Li, Y.-S., Lin, C.-Y., and Lee, J. J.:
520   Characterization and sources of aerosol particles over the southeastern Tibetan Plateau during the
521   Southeast Asia biomass-burning season, Tellus. B, 63, 117-128, 10.1111/j.1600-
522   0889.2010.00512.x, 2011.
523   Fang, K., Makkonen, R., Guo, Z., Zhao, Y., and Seppa, H.: An increase in the biogenic aerosol
524   concentration as a contributing factor to the recent wetting trend in Tibetan Plateau, Scientific
525   Reports, 5, 10.1038/srep14628, 2015.
526   Freney, E. J., Sellegri, K., Canonaco, F., Boulon, J., Hervo, M., Weigel, R., Pichon, J. M., Colomb, A.,
527   Prévôt, A. S. H., and Laj, P.: Seasonal variations in aerosol particle composition at the puy-de-
528   Dôme research station in France, Atmos. Chem. Phys., 11, 13047-13059, 10.5194/acp-11-13047-
529   2011, 2011.
530   Fröhlich, R., Crenn, V., Setyan, A., Belis, C. A., Canonaco, F., Favez, O., Riffault, V., Slowik, J. G., Aas,
531   W., Aijälä, M., Alastuey, A., Artiñano, B., Bonnaire, N., Bozzetti, C., Bressi, M., Carbone, C.,
532   Coz, E., Croteau, P. L., Cubison, M. J., Esser-Gietl, J. K., Green, D. C., Gros, V., Heikkinen, L.,
533   Herrmann, H., Jayne, J. T., Lunder, C. R., Minguillón, M. C., Močnik, G., O'Dowd, C. D.,
534   Ovadnevaite, J., Petralia, E., Poulain, L., Priestman, M., Ripoll, A., Sarda-Estève, R.,
535   Wiedensohler, A., Baltensperger, U., Sciare, J., and Prévôt, A. S. H.: ACTRIS ACSM
536   intercomparison – Part 2: Intercomparison of ME-2 organic source apportionment results from 15
537   individual, co-located aerosol mass spectrometers, Atmos. Meas. Tech., 8, 2555-2576,
538   10.5194/amt-8-2555-2015, 2015.
539   Giordano, M. R., Kalnajs, L. E., Avery, A., Goetz, J. D., Davis, S. M., and DeCarlo, P. F.: A missing
540   source of aerosols in Antarctica – beyond long-range transport, phytoplankton, and
541   photochemistry, Atmos. Chem. Phys., 17, 1-20, 10.5194/acp-17-1-2017, 2017.
542   Gu, Y., Liao, H., and Bian, J.: Summertime nitrate aerosol in the upper troposphere and lower stratosphere
543   over the Tibetan Plateau and the South Asian summer monsoon region, Atmos. Chem. Phys., 16,
544   6641-6663, 10.5194/acp-16-6641-2016, 2016.
545   He, Q. S., Li, C. C., Ma, J. Z., Wang, H. Q., Yan, X. L., Lu, J., Liang, Z. R., and Qi, G. M.: Lidar-observed
546   enhancement of aerosols in the upper troposphere and lower stratosphere over the Tibetan Plateau
547   induced by the Nabro volcano eruption, Atmos. Chem. Phys., 14, 11687-11696, 10.5194/acp-14-
548   11687-2014, 2014.
549   Heald, C. L., Kroll, J. H., Jimenez, J. L., Docherty, K. S., DeCarlo, P. F., Aiken, A. C., Chen, Q., Martin, S.
550   T., Farmer, D. K., and Artaxo, P.: A simplified description of the evolution of organic aerosol
551   composition in the atmosphere, Geophys. Res. Lett., 37, L08803, 10.1029/2010gl042737, 2010.
552   Jayne, J. T., Leard, D. C., Zhang, X., Davidovits, P., Smith, K. A., Kolb, C. E., and Worsnop, D. R.:
553   Development of an Aerosol Mass Spectrometer for Size and Composition Analysis of Submicron
554   Particles, Aerosol. Sci. Tech., 33, 49 - 70, http://dx.doi.org/10.1080/027868200410840, 2000.
555   Jimenez, J. L., Canagaratna, M. R., Donahue, N. M., Prevot, A. S. H., Zhang, Q., Kroll, J. H., DeCarlo, P.
556   F., Allan, J. D., Coe, H., Ng, N. L., Aiken, A. C., Docherty, K. S., Ulbrich, I. M., Grieshop, A. P.,
557   Robinson, A. L., Duplissy, J., Smith, J. D., Wilson, K. R., Lanz, V. A., Hueglin, C., Sun, Y. L.,
558   Tian, J., Laaksonen, A., Raatikainen, T., Rautiainen, J., Vaattovaara, P., Ehn, M., Kulmala, M.,
559   Tomlinson, J. M., Collins, D. R., Cubison, M. J., E., Dunlea, J., Huffman, J. A., Onasch, T. B.,
560   Alfarra, M. R., Williams, P. I., Bower, K., Kondo, Y., Schneider, J., Drewnick, F., Borrmann, S.,
561   Weimer, S., Demerjian, K., Salcedo, D., Cottrell, L., Griffin, R., Takami, A., Miyoshi, T.,
562   Hatakeyama, S., Shimono, A., Sun, J. Y., Zhang, Y. M., Dzepina, K., Kimmel, J. R., Sueper, D.,
563   Jayne, J. T., Herndon, S. C., Trimborn, A. M., Williams, L. R., Wood, E. C., Middlebrook, A. M.,
564   Kolb, C. E., Baltensperger, U., and Worsnop, D. R.: Evolution of Organic Aerosols in the
565   Atmosphere, Science, 326, 1525-1529, 10.1126/science.1180353, 2009.

566 Kroll, J. H., Donahue, N. M., Jimenez, J. L., Kessler, S. H., Canagaratna, M. R., Wilson, K. R., Altieri, K.
567   E., Mazzoleni, L. R., Wozniak, A. S., Bluhm, H., Mysak, E. R., Smith, J. D., Kolb, C. E., and
568   Worsnop, D. R.: Carbon oxidation state as a metric for describing the chemistry of atmospheric
569   organic aerosol, Nature Chem., 3, 133-139, 10.1038/nchem.948, 2011.
570 Kumar, R., Naja, M., Satheesh, S. K., Ojha, N., Joshi, H., Sarangi, T., Pant, P., Dumka, U. C., Hegde, P.,
571   and Venkataramani, S.: Influences of the springtime northern Indian biomass burning over the
572   central Himalayas, J. Geophys. Res.-Atmos., 116, 10.1029/2010jd015509, 2011.
573 Li, Z., Lau, W. K. M., Ramanathan, V., Wu, G., Ding, Y., Manoj, M. G., Liu, J., Qian, Y., Li, J., Zhou, T.,
574   Fan, J., Rosenfeld, D., Ming, Y., Wang, Y., Huang, J., Wang, B., Xu, X., Lee, S. S., Cribb, M.,
575   Zhang, F., Yang, X., Zhao, C., Takemura, T., Wang, K., Xia, X., Yin, Y., Zhang, H., Guo, J., Zhai,
576   P. M., Sugimoto, N., Babu, S. S., and Brasseur, G. P.: Aerosol and monsoon climate interactions
577   over Asia, Rev. Geophys., 54, 2015RG000500, 10.1002/2015RG000500, 2016.
578 Lin, M., Zhang, Z., Su, L., Hill-Falkenthal, J., Priyadarshi, A., Zhang, Q., Zhang, G., Kang, S., Chan, C.-Y.,
579   and Thiemens, M. H.: Resolving the impact of stratosphere-to-troposphere transport on the sulfur
580   cycle and surface ozone over the Tibetan Plateau using a cosmogenic 35S tracer, Journal of
581   Geophysical Research: Atmospheres, 121, 2015JD023801, 10.1002/2015JD023801, 2016.
582 Liu, B., Cong, Z., Wang, Y., Xin, J., Wan, X., Pan, Y., Liu, Z., Wang, Y., Zhang, G., Wang, Z., Wang, Y.,
583   and Kang, S.: Background aerosol over the Himalayas and Tibetan Plateau: observed
584   characteristics of aerosol mass loading, Atmos. Chem. Phys., 17, 449-463, 10.5194/acp-17-449-
585   2017, 2017.
586 Lu, Z., Streets, D. G., Zhang, Q., and Wang, S.: A novel back-trajectory analysis of the origin of black
587   carbon transported to the Himalayas and Tibetan Plateau during 1996–2010, Geophys. Res. Lett.,
588   39, L01809, 10.1029/2011gl049903, 2012.
589 Lüthi, Z. L., Škerlak, B., Kim, S. W., Lauer, A., Mues, A., Rupakheti, M., and Kang, S.: Atmospheric
590   brown clouds reach the Tibetan Plateau by crossing the Himalayas, Atmos. Chem. Phys., 15,
591   6007-6021, 10.5194/acp-15-6007-2015, 2015.
592 Marinoni, A., Cristofanelli, P., Laj, P., Duchi, R., Calzolari, F., Decesari, S., Sellegri, K., Vuillermoz, E.,
593   Verza, G. P., Villani, P., and Bonasoni, P.: Aerosol mass and black carbon concentrations, a two
594   year record at NCO-P (5079 m, Southern Himalayas), Atmos. Chem. Phys., 10, 8551-8562,
595   10.5194/acp-10-8551-2010, 2010.
596 Marinoni, A., Cristofanelli, P., Laj, P., Duchi, R., Putero, D., Calzolari, F., Landi, T. C., Vuillermoz, E.,
597   Maione, M., and Bonasoni, P.: High black carbon and ozone concentrations during pollution
598   transport in the Himalayas: Five years of continuous observations at NCO-P global GAW station,
599   Journal of Environmental Sciences, 25, 1618-1625, 10.1016/s1001-0742(12)60242-3, 2013.
600 Ng, N. L., Canagaratna, M. R., Jimenez, J. L., Chhabra, P. S., Seinfeld, J. H., and Worsnop, D. R.: Changes
601   in organic aerosol composition with aging inferred from aerosol mass spectra, Atmos. Chem. Phys.
602   Discuss., 11, 7095-7112, 10.5194/acpd-11-7095-2011, 2011.
603 Ortega, A. M., Day, D. A., Cubison, M. J., Brune, W. H., Bon, D., de Gouw, J. A., and Jimenez, J. L.:
604   Secondary organic aerosol formation and primary organic aerosol oxidation from biomass-burning
605   smoke in a flow reactor during FLAME-3, Atmos. Chem. Phys., 13, 11551-11571, 10.5194/acp-
606   13-11551-2013, 2013.
607 Paatero, P., and Tapper, U.: Positive matrix factorization: A non-negative factor model with optimal
608   utilization of error estimates of data values, Environmetrics, 5, 111-126, 10.1002/env.3170050203,
609   1994.
610 Rinaldi, M., Gilardoni, S., Paglione, M., Sandrini, S., Fuzzi, S., Massoli, P., Bonasoni, P., Cristofanelli, P.,
611   Marinoni, A., Poluzzi, V., and Decesari, S.: Organic aerosol evolution and transport observed at
612   Mt. Cimone (2165 m a.s.l.), Italy, during the PEGASOS campaign, Atmos. Chem. Phys., 15,
613   11327-11340, 10.5194/acp-15-11327-2015, 2015.
614 Ripoll, A., Minguillón, M. C., Pey, J., Jimenez, J. L., Day, D. A., Sosedova, Y., Canonaco, F., Prévôt, A. S.
615   H., Querol, X., and Alastuey, A.: Long-term real-time chemical characterization of submicron
616   aerosols at Montsec (southern Pyrenees, 1570 m a.s.l.), Atmos. Chem. Phys., 15, 2935-2951,
617   10.5194/acp-15-2935-2015, 2015.
618 Sang, X., Zhang, Z., Chan, C., and Engling, G.: Source categories and contribution of biomass smoke to
619   organic aerosol over the southeastern Tibetan Plateau, Atmospheric Environment, 78, 113-123,
620   10.1016/j.atmosenv.2012.12.012, 2013.

621   Schmale, J., Schneider, J., Nemitz, E., Tang, Y. S., Dragosits, U., Blackall, T. D., Trathan, P. N., Phillips,
622   G. J., Sutton, M., and Braban, C. F.: Sub-Antarctic marine aerosol: dominant contributions from
623   biogenic sources, Atmos. Chem. Phys., 13, 8669-8694, 10.5194/acp-13-8669-2013, 2013.
624   Shen, R. Q., Ding, X., He, Q. F., Cong, Z. Y., Yu, Q. Q., and Wang, X. M.: Seasonal variation of secondary
625   organic aerosol tracers in Central Tibetan Plateau, Atmos. Chem. Phys., 15, 8781-8793,
626   10.5194/acp-15-8781-2015, 2015.
627   Stockwell, C. E., Christian, T. J., Goetz, J. D., Jayarathne, T., Bhave, P. V., Praveen, P. S., Adhikari, S.,
628   Maharjan, R., DeCarlo, P. F., Stone, E. A., Saikawa, E., Blake, D. R., Simpson, I. J., Yokelson, R.
629   J., and Panday, A. K.: Nepal Ambient Monitoring and Source Testing Experiment (NAMaSTE):
630   emissions of trace gases and light-absorbing carbon from wood and dung cooking fires, garbage
631   and crop residue burning, brick kilns, and other sources, Atmos. Chem. Phys., 16, 11043-11081,
632   10.5194/acp-16-11043-2016, 2016.
633   Stone, E. A., Schauer, J. J., Pradhan, B. B., Dangol, P. M., Habib, G., Venkataraman, C., and Ramanathan,
634   V.: Characterization of emissions from South Asian biofuels and application to source
635   apportionment of carbonaceous aerosol in the Himalayas, J. Geophys. Res.-Atmos., 115,
636   10.1029/2009jd011881, 2010.
637   Sun, Y., Zhang, Q., Macdonald, A. M., Hayden, K., Li, S. M., Liggio, J., Liu, P. S. K., Anlauf, K. G.,
638   Leaitch, W. R., Steffen, A., Cubison, M., Worsnop, D. R., van Donkelaar, A., and Martin, R. V.:
639   Size-resolved aerosol chemistry on Whistler Mountain, Canada with a high-resolution aerosol
640   mass spectrometer during INTEX-B, Atmos. Chem. Phys., 9, 3095-3111, 10.5194/acp-9-3095-
641   2009, 2009.
642   Tang, M., and Reiter, E. R.: Plateau monsoons of the Northern Hemisphere: A comparison between North
643   America and Tibet, Monthly Weather Review, 112, 617-637, 1984.
644   Tobo, Y., Zhang, D., Iwasaka, Y., and Shi, G.: On the mixture of aerosols and ice clouds over the Tibetan
645   Plateau: Results of a balloon flight in the summer of 1999, Geophys. Res. Lett., 34, L23801,
646   10.1029/2007GL031132, 2007.
647   Ulbrich, I. M., Canagaratna, M. R., Zhang, Q., Worsnop, D. R., and Jimenez, J. L.: Interpretation of organic
648   components from Positive Matrix Factorization of aerosol mass spectrometric data, Atmos. Chem.
649   Phys., 9, 2891-2918, 10.5194/acp-9-2891-2009, 2009.
650   Van Damme, M., Erisman, J. W., Clarisse, L., Dammers, E., Whitburn, S., Clerbaux, C., Dolman, A. J.,
651   and Coheur, P. F.: Worldwide spatiotemporal atmospheric ammonia (NH3) columns variability
652   revealed by satellite, Geophys. Res. Lett., 42, 8660-8668, 2015.
653   Vernier, J. P., Thomason, L. W., and Kar, J.: CALIPSO detection of an Asian tropopause aerosol layer,
654   Geophys. Res. Lett., 38, L07804, 10.1029/2010GL046614, 2011.
655   Xu, C., Ma, Y. M., Panday, A., Cong, Z. Y., Yang, K., Zhu, Z. K., Wang, J. M., Amatya, P. M., and Zhao,
656   L.: Similarities and differences of aerosol optical properties between southern and northern sides
657   of the Himalayas, Atmos. Chem. Phys., 14, 3133-3149, 10.5194/acp-14-3133-2014, 2014.
658   Xu, J., Shi, J., Zhang, Q., Ge, X., Canonaco, F., Prévôt, A. S. H., Vonwiller, M., Szidat, S., Ge, J., Ma, J.,
659   An, Y., Kang, S., and Qin, D.: Wintertime organic and inorganic aerosols in Lanzhou, China:
660   sources, processes, and comparison with the results during summer, Atmos. Chem. Phys., 16,
661   14937-14957, 10.5194/acp-16-14937-2016, 2016.
662   Yanai, M., and Li, C.: Mechanism of heating and the boundary layer over the Tibetan Plateau, Monthly
663   Weather Review, 122, 305-323, 1994.
664   Zhang, Q., Jimenez, J. L., Canagaratna, M. R., Ulbrich, I. M., Ng, N. L., Worsnop, D. R., and Sun, Y.:
665   Understanding atmospheric organic aerosols via factor analysis of aerosol mass spectrometry: a
666   review, Anal. Bioanal. Chem., 401, 3045-3067, 10.1007/s00216-011-5355-y, 2011.
667   Zhang, R., Wang, H., Qian, Y., Rasch, P. J., Easter, R. C., Ma, P. L., Singh, B., Huang, J., and Fu, Q.:
668   Quantifying sources, transport, deposition, and radiative forcing of black carbon over the
669   Himalayas and Tibetan Plateau, Atmos. Chem. Phys., 15, 6205-6223, 10.5194/acp-15-6205-2015,
670   2015.
671   Zhang, R., Wang, Y., He, Q., Chen, L., Zhang, Y., Qu, H., Smeltzer, C., Li, J., Alvarado, L. M. A.,
672   Vrekoussis, M., Richter, A., Wittrock, F., and Burrows, J. P.: Enhanced trans-Himalaya pollution
673   transport to the Tibetan Plateau by cut-off low systems, Atmos. Chem. Phys., 17, 3083-3095,
674   10.5194/acp-17-3083-2017, 2017.
675   Zhao, Z., Cao, J., Shen, Z., Xu, B., Zhu, C., Chen, L. W. A., Su, X., Liu, S., Han, Y., Wang, G., and Ho, K.:
676   Aerosol particles at a high-altitude site on the Southeast Tibetan Plateau, China: Implications for

677   pollution transport from South Asia, J. Geophys. Res.-Atmos., 118, 11360-11375,
678   10.1002/jgrd.50599, 2013.
679   Zhou, S., Collier, S., Jaffe, D. A., Briggs, N. L., Hee, J., Sedlacek Iii, A. J., Kleinman, L., Onasch, T. B.,
680   and Zhang, Q.: Regional influence of wildfires on aerosol chemistry in the western US and
681   insights into atmospheric aging of biomass burning organic aerosol, Atmos. Chem. Phys., 17,
682   2477-2493, 10.5194/acp-17-2477-2017, 2017.

683

684

Table 1. Summary of AMS measurement at mountain sites around the world. The mass concentration was for NR-PM$_1$.

Sites	Instruments	Lat.	Long.	Elev.	Date	Mass Conc.	Reference
Nam Co	HR-AMS	30.77°N	90.9°E	4730	Jun-15	1.84	
Menyuan	ACSM	37.61°N	101.26°E	3925	5 September – 15 October, 2013	10.8	Du et al. (2015)
Montsec	ACSM	42.05°N	0.73°E	1570	14 July 2011 - 23 April 2012	4.9	Rinaldi et al. (2015)
Jungfraujoch	ToF-ACSM	46.55°N	07.98°E	3580	27 July 2012 - 2 October 2013	0.55	Fröhlich et al. (2015)
Mt. Cimone	HR-AMS	44.18°N	10.7°E	2165	June - July 2012	4.5	Rinaldi et al. (2015)
Mt. Whistler	HR-AMS	50.01°N	122.95°E	2182	Apr - May 2006	1.91	Sun et al. (2009)
Puy de Done	cToF-AMS	45.77°N	2.95°E	1465	Sep 2008 - June 2010	2008 Autumn: 7.82 2008 Winter: 5.58 2009 Summer: 27.594	Freney et al. (2011)
Mt. Bachelor	HR-AMS	43.98°S	121.69W	2800	25 July - 25 August, 2013	15.1	Zhou et al. (2017)
Sub-Antarctic Bird Island	HR-AMS	54.00°S	38.00°W	ND	November and December, 2010	0.46	Schmale et al. (2013)
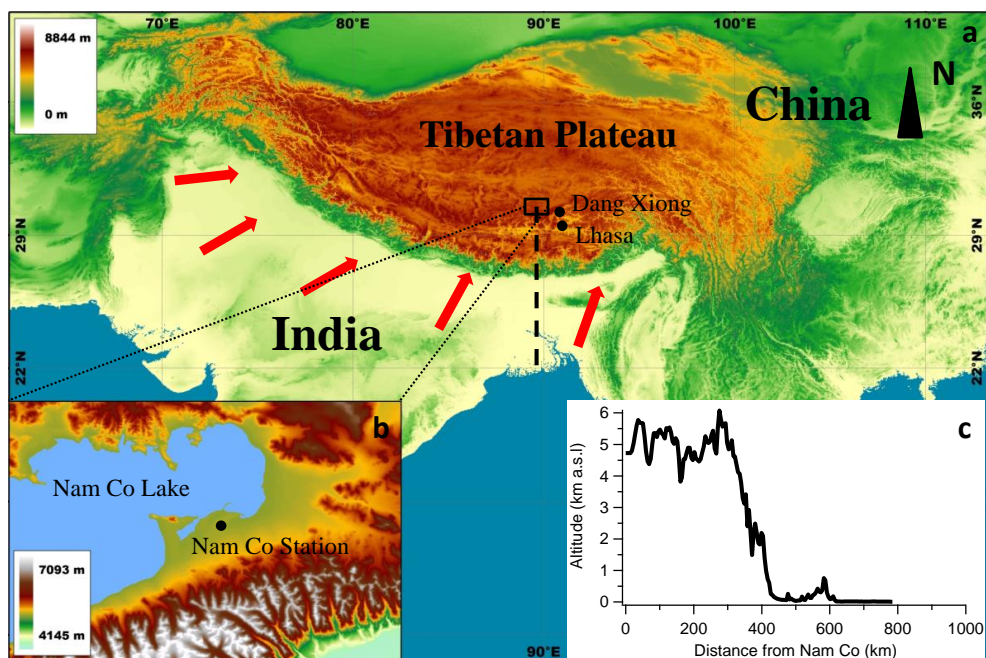
689

690   Figure 1. Location map for (a) the Tibetan Plateau and (b) Nam Co Station colored by the
691   elevation. (c) The elevation profile from costal area to Nam Co Station (vertical dash line). The
692   red arrow in the map represent the possible wind direction.

693

694
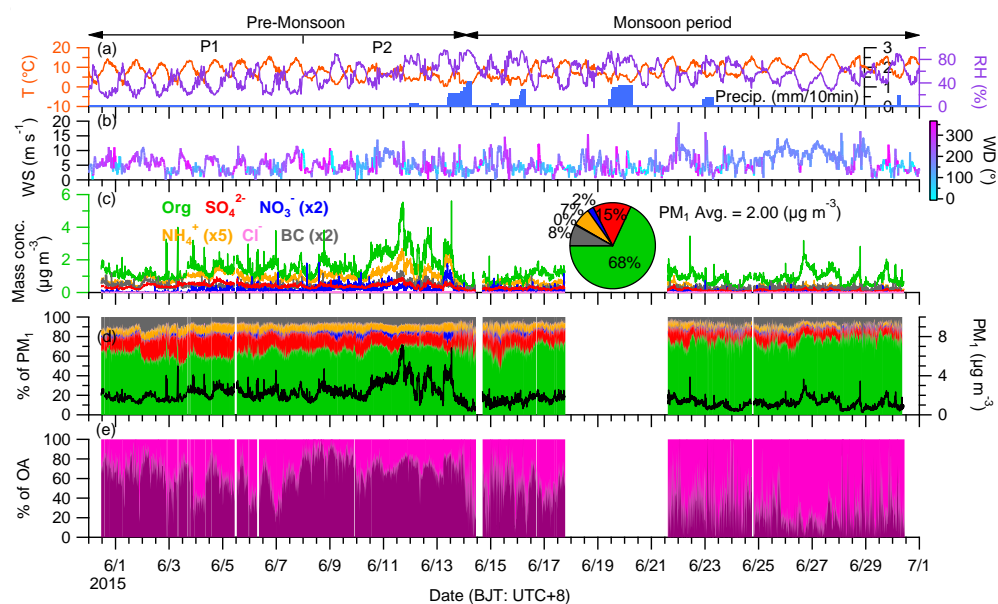
Figure 2. The combo plot of the data of the Nam Co study including (a) the meteorological conditions (T: air temperature; RH: relative humidity; Precip.: precipitation), (b) the variation of WS (wind speed) colored by WD (wind direction), (c) the temporal variation of mass concentration of PM_1 species and the average contribution each species (pie chart), (d) the mass contribution of each PM_1 species and the total mass concentration of PM_1, and (e) the mass contribution of PMF results (section 3.5). Three periods based on the meteorological conditions were marked.

702

703
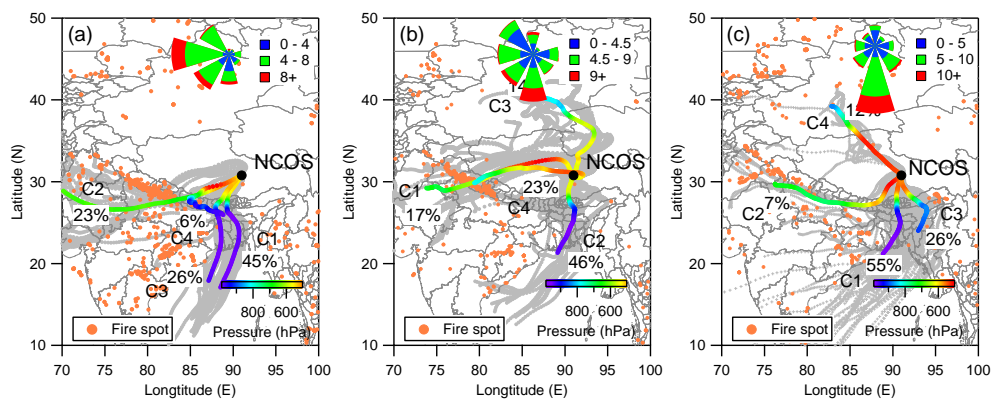
Figure 3. Air mass trajectory statistics for (a) P1, (b) P2, and (c) monsoon period. The classes of trajectories

are colored by pressure. Fire spot observed by MODIS and average wind rose plot during each period are

also shown.
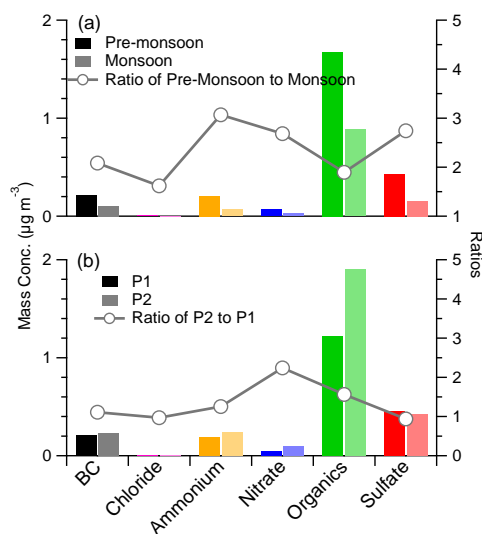
707

708   Figure 4. The comparisons of PM_1 species of the mass concentration (left axis) and the ratio between them

709   (right axis) between (a) pre-monsoon and monsoon and (b) P1 and P2.

710

711

712

713
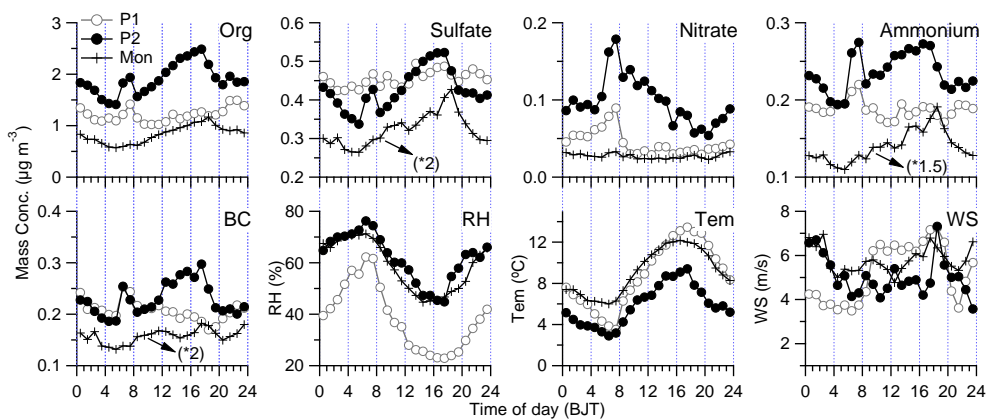
Figure 5. Diurnal variations of each species and weather conditions (RH: relative humidity; Tem: air temperature; and WS: wind speed) during three periods of the study. Note that the signals of sulfate, ammonium, and BC are increased by a factor for comparison.

717
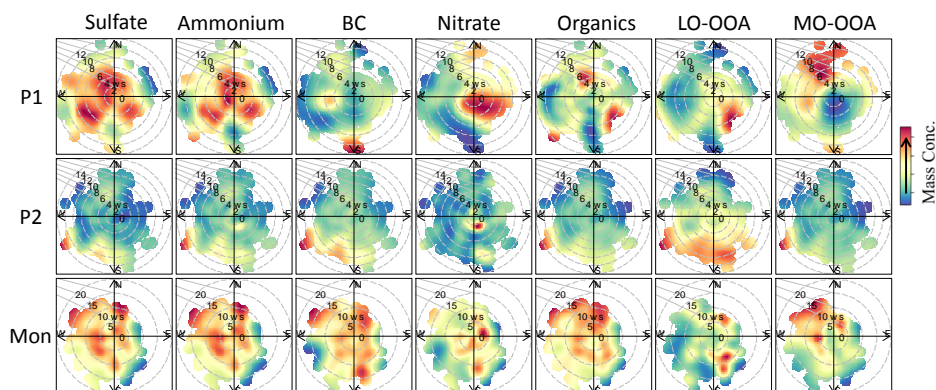
Figure 6. Bivariate polar plots that illustrate the variations of the concentrations (colored) of each species as a function of wind speed (m s^{-1}) and wind direction during different periods of the study.

718

719

720

721

722
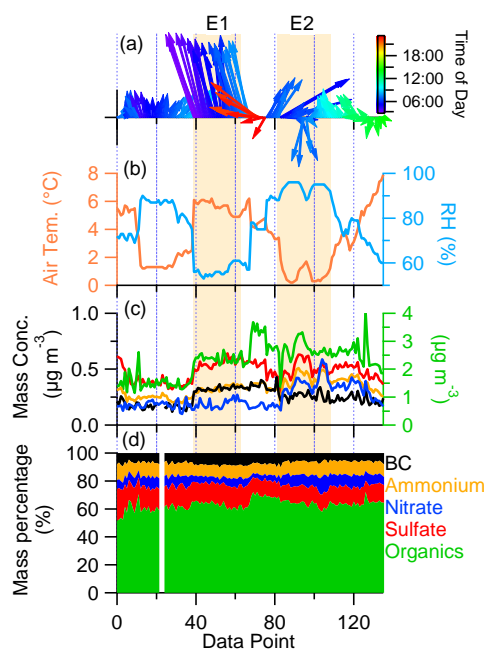
Figure 7. The high aerosol loading periods based on nitrate (> average + 2σ) accompanying with meteorological data.

725

Atmospheric
Chemistry
and Physics
Discussions

Open Access

726
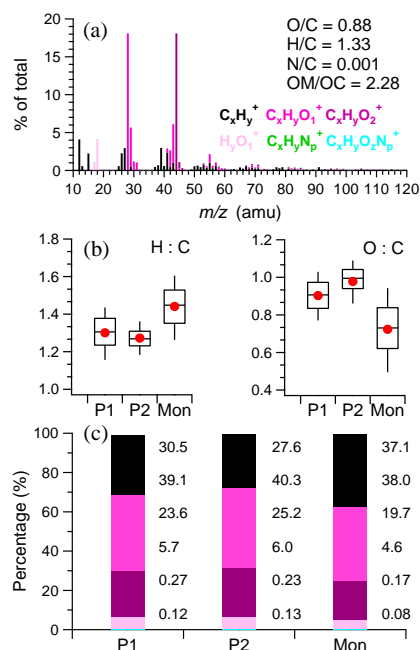
Figure 8. (a) The average mass spectrum of organic aerosol, (b) the average ratios of H : C and O : C

during different periods, and (c) the average contribution of six ion categories during different periods.

729

730

731
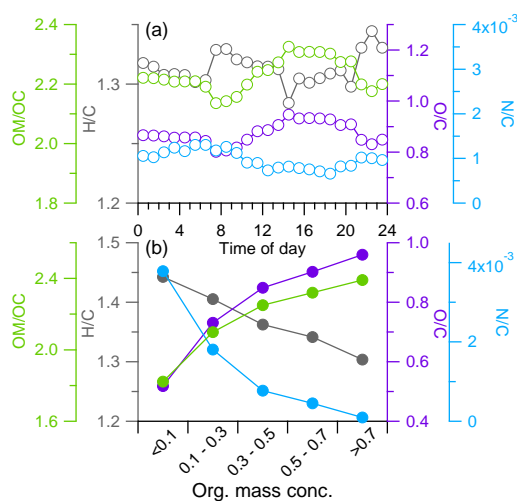
Figure 9. (a) Diurnal variations of elemental ratios and (b) the variations of elemental ratios as the function of mass concentration of organic aerosol.

Atmospheric
Chemistry
and Physics
Discussions

Open Access

EGU

736

737
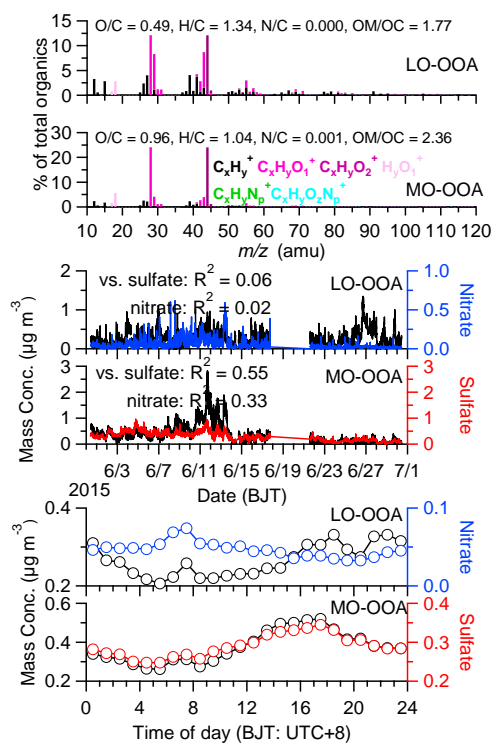
Figure 10. PMF results of (a) the mass spectra, (b) the temporal variation and (c) diurnal variations of two

factors. The temporal and diurnal variations of sulfate and nitrate are also shown for comparisons.

740

741

742
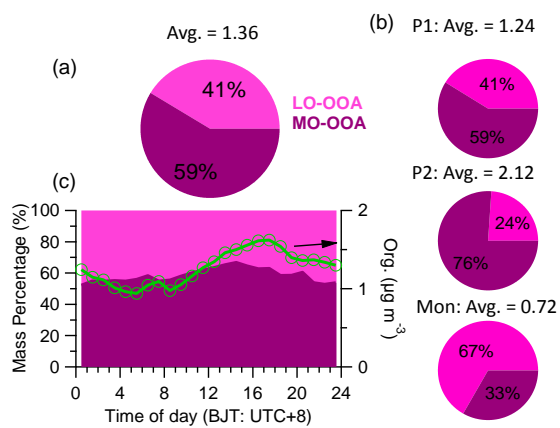
743

744 Figure 11. (a) The average mass contributions of two factors (a) during the study, (b) during the different

745 periods, and (c) the diurnal mass contribution of two factor (left axis) accompanying with the total organics

746 (right axis).

747
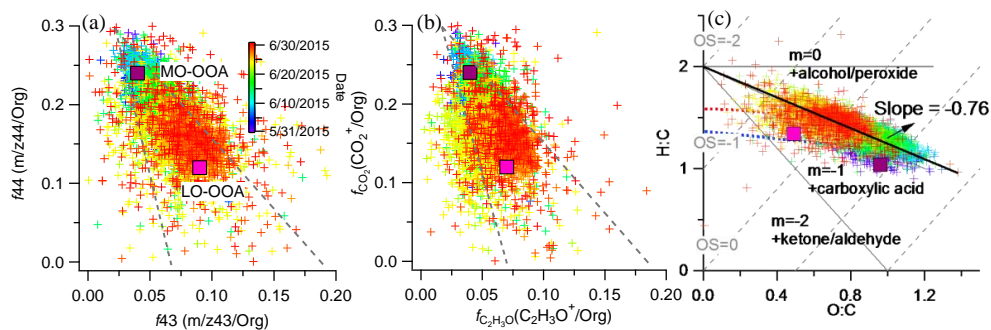
Figure 12. Scatter plots of (a) $f44$ vs. $f43$, (b) fCO_2^+ vs. $fC_2H_3O^+$, and (c) H:C vs. O:C for the OA. The corresponding values of the OOAs identified in this study are also shown.

Atmospheric
Chemistry
and Physics
Discussions

751
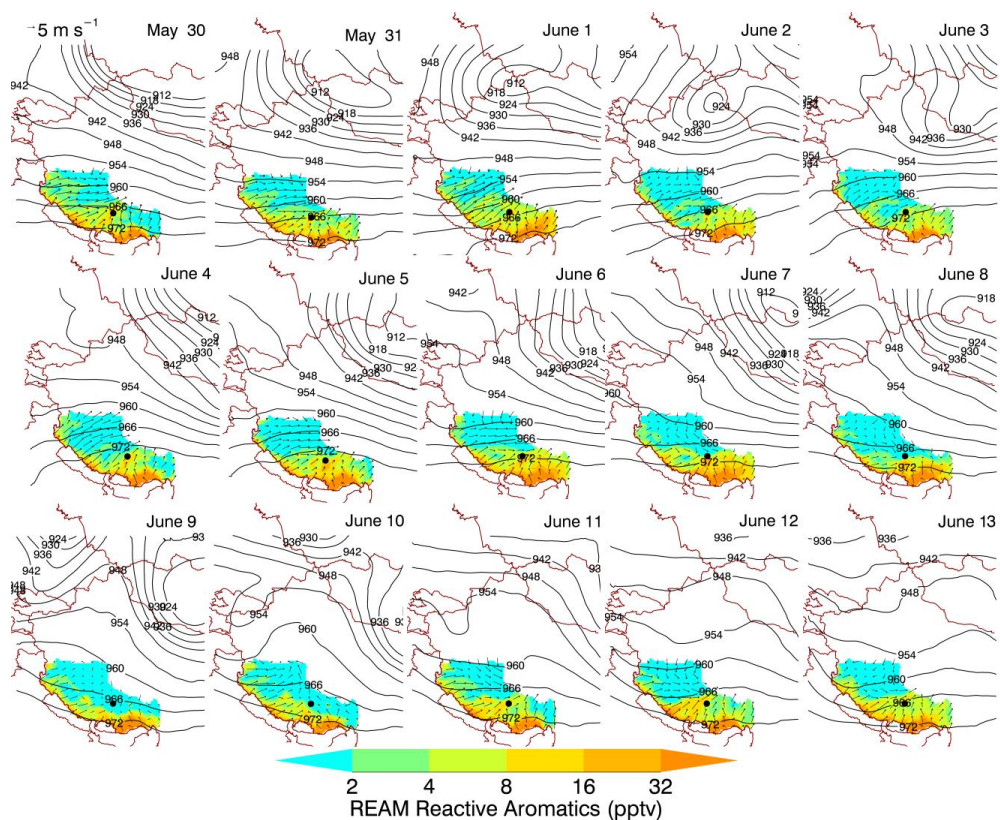
Figure 13. Daily distribution of WRF-simulated surface wind and REAM-simulated concentrations of reactive aromatics over the Tibet Plateau during 30 May to 13 June, 2015.

754